Wave functions of elliptical quantum dots in a magnetic field

Daming Zhou[a] and Axel Lorke[b]
Fakultät für Physik and CENIDE, Universität Duisburg-Essen, Lotharstraße 1, 47048 Duisburg, Germany

(Received 15 April 2014; accepted 9 October 2014)

We use the variational principle to obtain the wave functions of elliptical quantum dots under the influence of an external magnetic field. For the first excited states, whose wave functions have recently been mapped experimentally, we find a simple expression, based on a linear combination of the wave functions in the absence of a magnetic field. The results illustrate how a magnetic field breaks the *x*-*y* symmetry and mixes the corresponding eigenstates. The obtained eigenenergies agree well with those obtained by more involved analytical and numerical methods.

[http://dx.doi.org/10.1119/1.4898790]

I. INTRODUCTION

Semiconductor technologies, such as crystal growth and lithography, have been improving continually over the past decades. As a result, it is possible today to reliably fabricate semiconductor structures that have sizes of only around 10 nm in all spatial dimensions. For typical doping densities, only very few carriers (electrons or holes) will be present in these nano-structures, and therefore, their charge quantization will be apparent. Furthermore, the carriers can no longer be treated as classical point charges, because they are confined to a region of space that is smaller than the de Broglie wavelength in bulk semiconductors. A full quantum approach is needed in order to unravel the energy spectra in such three-dimensional semiconductor nanostructures, which are called "quantum dots" for short. Quantum dots can be fabricated with different sizes and shapes, so that their energy structure (and thus their electronic and optical properties) can be tailored to match desired specifications. This flexibility makes quantum dots attractive for a wide range of applications, from solar cells to lasers, and products such as quantum dot LCD displays have just entered the consumer market.[1]

On the other hand, quantum dots have always sparked the interest of basic science, as they are ideal model systems to study the many-particle interactions of confined carriers. In this respect, they share many similarities with electrons confined in the Coulomb potential of atoms, and many of the basic properties and phenomena of atomic physics can also be found in quantum dots. Examples are a distinct shell structure,[2] direct Coulomb interaction and exchange interaction,[3] incomplete shell filling,[4] orbital Zeemann splitting,[5] and the (quantum confined) Stark effect.[6] Therefore, quantum dots are sometimes referred to as "artificial atoms."

Contrary to real atoms, however, it is practical to apply external fields to quantum dots that compete in strength with the "built-in" confining potential. To illustrate this, consider that in order to match the magnetic energy (Landau level spacing) with the Rydberg energy of a hydrogen atom, a magnetic field of 10^5 T would be required—many orders of magnitude above anything achievable in the laboratory. For quantum dots, on the other hand, a comparable situation is reached at moderate fields of 1–10 T. Therefore, the application of a magnetic field is not just a small perturbation—it can profoundly modify the quantum states and the energy structure of the quantum dots.[3]

One type of quantum dot that has attracted particular attention is the so-called self-assembled quantum dot.[7] These structures form when a thin layer of a suitable semiconductor (commonly InAs) is deposited on an appropriate substrate of a different semiconductor (commonly GaAs). In the so-called Stranski-Krastanov growth mode, the top layer will form a random array of nanoscopic islands, which can be overgrown by the substrate material without breaking the integrity of the crystal lattice. When the island material has a lower conduction band energy than the matrix, the islands will constitute an attractive potential for electrons and thus serve as quantum dots. The confining potential in self-assembled quantum dots is smooth. And even though its detailed shape is given by a complex interplay between the potential of external charges, band bending, strain, and piezoelectric fields, it can be well approximated using a simple two-dimensional harmonic oscillator ansatz.[8] Therefore, these quantum dots are not only a topic of great interest in basic and applied physics, they also provide the advanced student with a number of interesting but manageable problems in quantum mechanics, with direct connections to contemporary physics research.

In the following, we will use the harmonic oscillator model to investigate how the interplay between the internal confining potential and an external magnetic field gives rise to a tunable mixing of wave functions. Such a controlled modification of the wave functions has recently been observed experimentally,[9,10] so that this example of a variational ansatz provides a direct link to contemporary nanoscience.

The treatment of the isotropic two-dimensional harmonic oscillator, which can be found in many textbooks,[11] can easily be extended to also include a magnetic field that is applied perpendicular to the plane of the two-dimensional oscillator. If, however, an anisotropic contribution breaks the circular symmetry of the potential,[9,10] the derivation of the energy levels and wave functions in a magnetic field becomes more involved. It is the purpose of this work to show that a straightforward application of the variational method leads to simple expressions for the wave functions and energies of an anisotropic harmonic oscillator in a magnetic field. These expressions nevertheless approximate the exact results with high accuracy.

II. VARIATIONAL METHOD

We assume that the confining potential is in the *xy*-plane and the magnetic field points along the *z*-axis. The Hamiltonian can be written in the form[11]

$$H = \frac{1}{2m}(\vec{p} + e\vec{A})^2 + V, \tag{1}$$

where m is the effective electronic mass, $\vec{A}$ is the vector potential of the magnetic field, and V is the two-dimensional confining potential

$$V(x,y) = \frac{1}{2}m\omega_x^2 x^2 + \frac{1}{2}m\omega_y^2 y^2. \tag{2}$$

When the two characteristic frequencies are different ($\omega_x \neq \omega_y$), this potential describes an anisotropic harmonic oscillator. Choosing the symmetric gauge[12] $A_x = -By/2$, $A_y = Bx/2$, $A_z = 0$, we obtain for the Hamiltonian

$$\begin{aligned} H &= \frac{1}{2m}\left[\left(\hat{p}_x - \frac{eBy}{2}\right)^2 + \left(\hat{p}_y + \frac{eBx}{2}\right)^2\right] \\ &\quad + \frac{1}{2}m\omega_x^2 x^2 + \frac{1}{2}m\omega_y^2 y^2 \\ &= \frac{\hat{p}_x^2}{2m} + \frac{1}{2}m\omega_1^2 x^2 + \frac{\hat{p}_y^2}{2m} + \frac{1}{2}m\omega_2^2 y^2 \\ &\quad + \frac{eB}{2m}\left(x\hat{p}_y - y\hat{p}_x\right) = H_1 + \frac{1}{2}\omega_c \hat{l}_z. \end{aligned} \tag{3}$$

Here, we have used the abbreviations $H_1 = \hat{p}_x^2/2m + m\omega_1^2 x^2/2 + \hat{p}_y^2/2m + m\omega_2^2 y^2/2$, $\omega_1 = \sqrt{\omega_x^2 + \omega_c^2/4}$, and $\omega_2 = \sqrt{\omega_y^2 + \omega_c^2/4}$. Furthermore, $\hat{l}_z = x\hat{p}_y - y\hat{p}_x$ is the orbital angular momentum along the z-direction and $\omega_c = eB/m$ is the cyclotron frequency. For later convenience, we also introduce the length normalization parameters $\alpha_1 = \sqrt{m\omega_1/\hbar}$ and $\alpha_2 = \sqrt{m\omega_2/\hbar}$.

When no magnetic field is applied ($B = 0$), the Hamiltonian can be separated in x and y, and the eigenfunctions $\psi_{n_x,n_y}(x,y)$ are easily found as products of the well-known wave functions of the one-dimensional harmonic oscillators. The corresponding energies are $E_{n_x,n_y} = \hbar\omega_x(n_x + 1/2) + \hbar\omega_y(n_y + 1/2)$. In the following, we will restrict ourselves to the discussion of the so-called "p-states,"[13] with $(n_x, n_y) = (1,0)$ or $(0,1)$, because they exhibit an interesting change in topology when the magnetic field is turned on, and because they have recently been mapped out experimentally.[9,10] For these states and $B = 0$, the energies and the wave functions are

$$\begin{aligned} E_{10} &= \frac{3}{2}\hbar\omega_x + \frac{1}{2}\hbar\omega_y, \\ \psi_{10} &= \sqrt{\frac{2\alpha_1\alpha_2}{\pi}}\alpha_1 x e^{-\left(\alpha_1^2x^2 + \alpha_2^2y^2\right)/2}, \end{aligned} \tag{4}$$

$$\begin{aligned} E_{01} &= \frac{1}{2}\hbar\omega_x + \frac{3}{2}\hbar\omega_y, \\ \psi_{01} &= \sqrt{\frac{2\alpha_1\alpha_2}{\pi}}\alpha_2 y e^{-\left(\alpha_1^2x^2 + \alpha_2^2y^2\right)/2}. \end{aligned} \tag{5}$$

For $B \neq 0$, the Hamiltonian is no longer separable, because the angular momentum term $\omega_c\hat{l}_z/2$ in Eq. (3) mixes the x and y directions. For very high magnetic fields, on the other hand, the anisotropy will no longer be relevant $(\omega_1, \omega_2 \approx \omega_c/2)$ and the wave functions can be written in cylindrical coordinates (r, φ) as

$$\psi^{\pm}(r,\varphi) = \frac{1}{\sqrt{\pi}l^2}\, r e^{-r^2/2l^2}\, e^{\pm i\varphi}, \tag{6}$$

where $x^2 + y^2 = r^2$, $l^2 = \hbar/(m\omega_c)$, and $x + iy = re^{i\varphi}$.

Guided by the fact that both limiting cases $B = 0$ and $B \to \infty$ can be solved exactly, we use a simple linear combination of ψ_{10} and ψ_{01} as a trial function to make a variational approximation over the whole range of magnetic fields

$$\psi = a\psi_{10} + ib\psi_{01}. \tag{7}$$

Here, a is a real number between 0 and 1, and $b = \pm\sqrt{1-a^2}$ to ensure normalization of ψ. To minimize the energy with respect to a, we calculate the expectation value of ψ,

$$E = \langle\psi|H|\psi\rangle = \left\langle a\psi_{10} + ib\psi_{01}\middle| H_1 + \frac{1}{2}\omega_c\hat{l}_z\middle| a\psi_{10} + ib\psi_{01}\right\rangle. \tag{8}$$

Using the fact that $|\psi_{10}\rangle$ and $|\psi_{01}\rangle$ are eigenstates of H_1 with energies given by Eqs. (4) and (5), we find for the first part of the Hamiltonian in Eq. (8),

$$\begin{aligned} &\langle a\psi_{10} + ib\psi_{01}|H_1|a\psi_{10} + ib\psi_{01}\rangle \\ &\quad = a^2\left(\frac{3}{2}\hbar\omega_1 + \frac{1}{2}\hbar\omega_2\right) + b^2\left(\frac{1}{2}\hbar\omega_1 + \frac{3}{2}\hbar\omega_2\right). \end{aligned} \tag{9}$$

To find the angular momentum contribution in Eq. (8), we first calculate

$$\begin{aligned} \hat{l}_z|\psi_{10}\rangle &= \left(x\hat{p}_y - y\hat{p}_x\right)|\psi_{10}\rangle = -i\hbar\left(x\frac{\partial\psi_{10}}{\partial y} - y\frac{\partial\psi_{10}}{\partial x}\right) \\ &= -i\hbar\left[\left(\alpha_1^2 - \alpha_2^2\right)xy - \frac{y}{x}\right]\psi_{10} \\ &= -i\hbar\left[\left(\alpha_1^2 - \alpha_2^2\right)x^2 - 1\right]\frac{\alpha_1}{\alpha_2}\psi_{01}, \end{aligned} \tag{10}$$

from which it follows that

$$\begin{aligned} \langle\psi_{01}|\hat{l}_z|\psi_{10}\rangle &= \langle\psi_{01}| - i\hbar\left[\left(\alpha_1^2 - \alpha_2^2\right)x^2 - 1\right]\frac{\alpha_1}{\alpha_2}|\psi_{01}\rangle \\ &= i\hbar\frac{\alpha_1}{\alpha_2} - i\hbar\left(\alpha_1^2 - \alpha_2^2\right)\frac{\alpha_1}{\alpha_2}\langle\psi_{01}|x^2|\psi_{01}\rangle \\ &= i\hbar\frac{\alpha_1^2 + \alpha_2^2}{2\alpha_1\alpha_2}. \end{aligned} \tag{11}$$

Here, we have used $\langle\psi_{01}|x^2|\psi_{01}\rangle = 1/(2\alpha_1^2)$. The term $\langle\psi_{10}|\hat{l}_z|\psi_{01}\rangle$ can be derived from

$$\langle\psi_{10}|\hat{l}_z|\psi_{01}\rangle = \langle\psi_{01}|\hat{l}_z|\psi_{10}\rangle^{\dagger} = -i\hbar\frac{\alpha_1^2 + \alpha_2^2}{2\alpha_1\alpha_2}. \tag{12}$$

Because ψ_{10} and ψ_{01} are eigenstates of the Hamiltonian of *linear* motion (H_1, separable in x and y), their angular momentum expectation value is zero: $\langle\psi_{10}|\hat{l}_z|\psi_{10}\rangle = \langle\psi_{01}|\hat{l}_z|\psi_{01}\rangle = 0$.

Combining the above results, we calculate the angular momentum contribution to E in Eq. (8) to be

$$\begin{aligned} &\left\langle a\psi_{10} + ib\psi_{01}\middle|\frac{1}{2}\omega_c\hat{l}_z\middle|a\psi_{10} + ib\psi_{01}\right\rangle \\ &\quad = \frac{1}{2}ab\,\hbar\omega_c\frac{\alpha_1^2 + \alpha_2^2}{\alpha_1\alpha_2} \\ &\quad = \frac{1}{2}ab\,\hbar\omega_c\frac{\omega_1 + \omega_2}{\sqrt{\omega_1\omega_2}}, \end{aligned} \tag{13}$$

and thus obtain the total energy

$$E = a^2\left(\frac{3}{2}\hbar\omega_1 + \frac{1}{2}\hbar\omega_2\right) + b^2\left(\frac{1}{2}\hbar\omega_1 + \frac{3}{2}\hbar\omega_2\right) + \frac{1}{2}ab\,\hbar\omega_c\frac{\omega_1+\omega_2}{\sqrt{\omega_1\omega_2}}. \tag{14}$$

In order to find the minimum energy, we take the derivative with respect to a of Eq. (14), using $b = \pm\sqrt{1-a^2}$,

$$\frac{\partial E}{\partial a} = 2a(\hbar\omega_1 - \hbar\omega_2) \pm \frac{1-2a^2}{2\sqrt{1-a^2}}\,\hbar\omega_c\frac{\omega_1+\omega_2}{\sqrt{\omega_1\omega_2}} = 0 \tag{15}$$

$$\Rightarrow \frac{\pm a\sqrt{1-a^2}}{2a^2-1} = \frac{\omega_c}{4(\omega_1-\omega_2)}\frac{\omega_1+\omega_2}{\sqrt{\omega_1\omega_2}}. \tag{16}$$

For simplicity, we define a parameter β, which characterizes the anisotropy and also accounts for the applied magnetic field

$$\beta = \frac{\omega_c}{4(\omega_1-\omega_2)}\frac{\omega_1+\omega_2}{\sqrt{\omega_1\omega_2}}. \tag{17}$$

The variational parameters are then easily computed in terms of β, giving

$$a_\pm^2 = \frac{1}{2} \pm \sqrt{\frac{1}{16\beta^2+4}}, \tag{18}$$

$$b_\pm^2 = \frac{1}{2} \mp \sqrt{\frac{1}{16\beta^2+4}}. \tag{19}$$

The sign (positive or negative) of the root of b^2 in Eq. (19) needs to be chosen to correctly reflect the chirality of the solutions with respect to the magnetic field. For $\omega_x > \omega_y$ and $B > 0$, the sign will be the same as the one on the right hand side of Eq. (18).

Let us now consider a few limiting cases. For $\omega_c \to 0$, we find $a_+ \to 1$, $E^+ \to 3/2\hbar\omega_x + 1/2\hbar\omega_y$, and $a_- \to 0$, $E^- \to 1/2\hbar\omega_x + 3/2\hbar\omega_y$; while for $\omega_c \to \infty$ we have $a_\pm \to 1/\sqrt{2}$, $b_\pm \to 1/\sqrt{2}$, $E^+ \to 3/2\hbar\omega_c$, $E^- \to 1/2\hbar\omega_c$. These results are in agreement with the two lowest Landau levels, into which the two p-states merge at high fields.[12] Furthermore, for a symmetric dot with $\omega_x = \omega_y = \omega$, we obtain $E^\pm = 2\hbar\sqrt{\omega^2 + \omega_c^2/4} \pm \hbar\omega_c/2$, the exact result for the well-known energies of the rotationally symmetric parabolic confinement.

III. CALCULATED RESULTS AND DISCUSSION

We can now directly compare our calculations with recent experimental and theoretical results on self-assembled InAs quantum dots.[9,10] Note that the wave functions in Refs. 9 and 10 were calculated numerically. We consider the $p^\pm$ states for different magnetic fields (1, 3, and 9 T), using parameters that are appropriate for the experimentally investigated self-assembled InAs quantum dots: $\hbar\omega_x = 62.9$ meV, $\hbar\omega_y = 56.9$ meV, and $m = 0.07m_e$.

The calculated probability densities $|\psi^\pm|^2$ are shown in Fig. 1. Here, the x and y axes are oriented horizontally and vertically, respectively, and run through the center of each panel. First, we focus on the higher-energy p^+ state. From Eq. (4), we see that at $B = 0$ this state has a node along the $x = 0$ line ($\psi_{10}(0, y) = 0$). The nodal structure is well preserved at a low magnetic field $B = 1$ T, as seen in the top left panel of Fig. 1. This is because $\omega_c \ll |\omega_1 - \omega_2|$, resulting in $|\beta| \ll 1$ and so, according to Eqs. (18) and (19), $(a, b) \approx (1, 0)$, which gives the original wave function ψ_{10}. With increasing magnetic field, β increases and the wave functions become more and more mixed. Roughly speaking, the magnetic force imposes a stronger and stronger circular symmetry onto the p^+ state, so that the node along the y-axis gives way to a more ring-like shape of the wave function. For the p^- state, a very similar development is observed. In the experimentally investigated range $B \leq 9$ T, the states will only partly develop a ring shape, with superimposed maxima along the rim, which are remnants of the lobes of ψ_{10} and ψ_{01}.

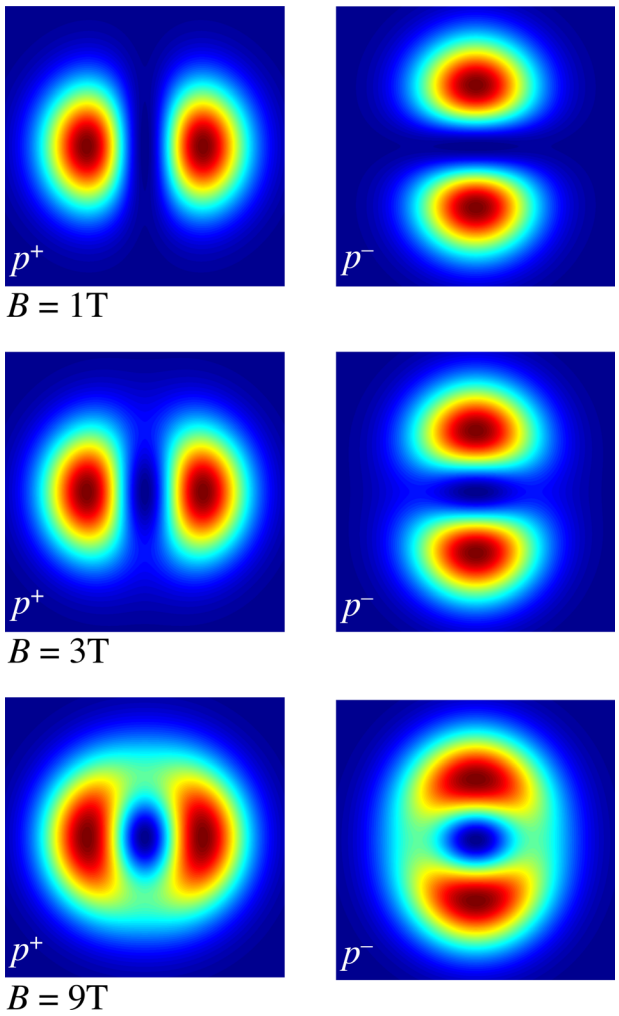

Fig. 1. Calculated probability densities for the p-state wave functions of a two-dimensional elliptical quantum dot in a perpendicular magnetic field. With increasing magnetic field, the nodal structure of the wave functions gives way to a more circular, ring-like shape.

The corresponding energy diagram is shown in Fig. 2. Due to different confinement energies in the x and y directions, the two p-state energies separate at zero magnetic field, with an energy gap between E^+ and E^-. The inset in Fig. 2 compares the energies of elliptical and circular quantum dots. With increasing magnetic fields, the energies of the $p^\pm$ states merge with those of a symmetric quantum dot: the

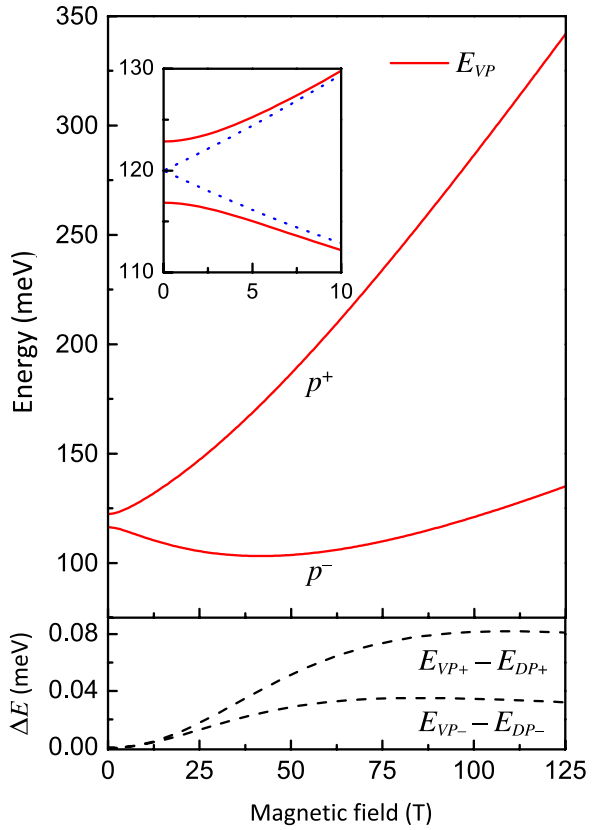

Fig. 2. Calculated energies for the p states, using a model potential with $\hbar\omega_x = 62.9$ meV and $\hbar\omega_y = 56.9$ meV. The inset compares the energies of an elliptical (solid line) and a symmetric (dotted line) quantum dot. The lower panel shows the deviation between the variational ansatz (E_{VP}) and an exact calculation (E_{DP}).

broken symmetry of the elongated dot is superseded by the circular symmetry imposed by the magnetic force.

Additionally, we compare our calculated energies to the exact eigenenergies given in Refs. 14 and 15: $E_{n_+,n_-} = (n_+ + 1/2)\hbar\omega^+ + (n_- + 1/2)\hbar\omega^-$, where the quantum numbers (n_+, n_-) are (1,0) and (0,1) for the p^+ and p^- states, respectively, and

$$\omega^{\pm} = \frac{1}{\sqrt{2}}\{(\omega_x^2 + \omega_y^2 + \omega_c^2) \pm [(\omega_x^2 + \omega_y^2 + \omega_c^2)^2 - 4\omega_x^2\omega_y^2]^{1/2}\}^{1/2}. \quad (20)$$

The difference between the two results, plotted in the lower panel of Fig. 2, shows that the deviations are of the order of one percent. (On the scale of the upper part of Fig. 2, the two dispersions are indistinguishable from each other.) As expected from a variational approach, our calculated energies are always somewhat higher than the exact results. As pointed out above, the variational ansatz gives exact results for zero magnetic field, and for $B \to \infty$. This can also be seen in the bottom of Fig. 2, where the deviation is zero at $B = 0$, then reaches a maximum and finally decreases again for very high magnetic fields.

IV. COMPARISON WITH EXPERIMENTAL DATA

The mixing of wave functions in elliptical quantum dots has recently been studied using magneto-tunneling spectroscopy. With this technique, the probability density is sampled in momentum space rather than in real space. Fortunately, a peculiarity of the harmonic oscillator is the fact that (apart from pre-factors) its Hamiltonian is the same in both real and momentum space. Basically, the harmonic oscillator wave functions are their own Fourier transforms. The wave functions (4) and (5) can therefore easily be expressed in reciprocal space by making the substitutions $x \to k_x$, $y \to k_y$, $\alpha_1 \to 1/\alpha_1$, and $\alpha_2 \to 1/\alpha_2$, to obtain

$$\psi_{10}(k_x, k_y) = \sqrt{\frac{2}{\alpha_1\alpha_2\pi}}\,\frac{k_x}{\alpha_1}\exp\left(-\frac{k_x^2}{2\alpha_1^2} - \frac{k_y^2}{2\alpha_2^2}\right), \quad (21)$$

$$\psi_{01}(k_x, k_y) = \sqrt{\frac{2}{\alpha_1\alpha_2\pi}}\,\frac{k_y}{\alpha_2}\exp\left(-\frac{k_x^2}{2\alpha_1^2} - \frac{k_y^2}{2\alpha_2^2}\right). \quad (22)$$

Because of the linearity of the Fourier transform, the dimensionless mixing parameters a and b will be the same in both representations.

In order to compare our calculation with the experimental data, we take $\hbar\omega_x = 62.9$ meV, $\hbar\omega_y = 56.9$ meV, and $m = 0.07m_e$ (from Ref. 10) and obtain for the variational parameters $a = 1$, $b = 0$ for $B = 0$ T and $a = 0.8280$, $b = 0.5607$ for $B = 9$ T. The resulting calculated probability density is shown as a contour plot in Fig. 3 (right). At $B = 9$ T, because $a > b$, the wave function is still dominated by the nodal structure of ψ_{10} (with nodes along the x-axis). On the other hand, because $b > 0$, we can already observe the influence of the magnetic field, giving the probability density a "volcano"-like shape. These features are in good agreement with the experimental data, shown in Fig. 3 (left). However, there are also some differences between the experiment and the calculation. The experimental data cover a wider range in k-space and seems to be more

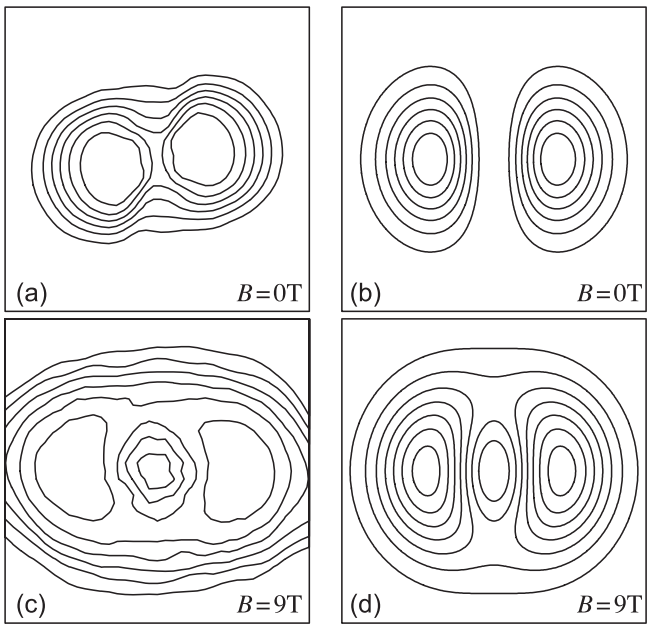

Fig. 3. Left: Experimental map of the probability density in momentum space of the p^+ state in self-organized quantum dots at a magnetic field of 0 and 9 T (Ref. 10). Right: Calculated quantum dot wave functions in k-space. The plots span a momentum range of $-5.8 \times 10^8\ \mathrm{m}^{-1} \le k_x, k_y \le +5.8 \times 10^8\ \mathrm{m}^{-1}$.

asymmetric. This can be attributed to an uncertainty regarding two experimental parameters: (1) the tunneling distance, which is needed in magneto-tunneling spectroscopy to convert the applied in-plane magnetic field into a momentum shift (a thicker barrier would shrink the experimental density plot); and (2) the exact shape anisotropy of the dots, which was assumed to be about $\pm 5\%$[10] (in other experiments, a more pronounced anisotropy has been observed[16]). Finally, the two maxima along the x-direction as well as the minimum in the center appear less pronounced in the experimental data than in the calculated density plots. This can be understood as a result of the limited experimental resolution, caused by the size and shape distribution of the investigated dot ensemble and by the admixture of tunneling current from states in the back contact with non-vanishing angular momentum, as discussed in Ref. 10. All in all, the calculated probability density can well reproduce all characteristic features of states in elliptical quantum dots that are subjected to a perpendicular magnetic field that mixes the $B = 0$ eigenstates.

V. CONCLUSION

We have used a variational approach to model the wave functions in a quantum dot with an elongated, parabolic confinement, subjected to a magnetic field. Simple expressions are found for both the energies and the wave functions of the first excited states, which very well approximate the numerical and analytic results given in other work. Our calculations are an instructive example of how to apply the variational principle to understand recent results in basic physics. Furthermore, these simple expressions, derived from the wave functions of the unperturbed, circular quantum dot, may also facilitate analytic calculations of the direct and exchange Coulomb interactions, which have been used successfully for circular quantum dots.[17]

ACKNOWLEDGMENTS

The authors would like to thank Christian Notthoff for fruitful discussions and acknowledge financial support by the project "Hochfunktionale Speicher (HOFUS)" within the VIP program of the BMBF. D. Zhou would like to thank the China Scholarship Council (CSC) for financial support.

[a]On leave from Shanghai Advanced Research Institute, Chinese Academy of Sciences, No. 99 Haike Road, Zhangjiang Hi-Tech Park, Pudong, Shanghai 201203, China.
[b]Electronic mail: axel.lorke@uni-due.de

[1]K. Bourzac, "Quantum dots go on display," Nature **493**, 283 (2013).
[2]P. M. Petroff, A. Lorke, and A. Imamoglu, "Epitaxially self-assembled quantum dots," Phys. Today **54**(5), 46–52 (2001).
[3]S. Tarucha, D. G. Austing, T. Honda, R. J. van der Hage, and L. P. Kouwenhoven, "Shell filling and spin effects in a few electron quantum dot," Phys. Rev. Lett. **77**(17), 3613–3616 (1996).
[4]D. Reuter, P. Kailuweit, A. D. Wieck, U. Zeitler, O. S. Wibbelhoff, C. Meier, A. Lorke, and J. C. Maan, "Coulomb-interaction induced incomplete shell filling in the hole system of self-assembled InAs quantum dots," Phys. Rev. Lett. **94**, 026808 (2005).
[5]H. Drexler, D. Leonard, W. Hansen, J. P. Kotthaus, and P. M. Petroff, "Spectroscopy of quantum levels in charge-tunable InGaAs quantum dots," Phys. Rev. Lett. **73**(16), 2252–2255 (1994).
[6]B. Alén, F. Bickel, K. Karrai, R. J. Warburton, and P. M. Petroff, "Stark-shift modulation absorption spectroscopy of single quantum dots," Appl. Phys. Lett. **83**(11), 2235–2237 (2003).
[7]B. J. Riel, "An introduction to self-assembled quantum dots," Am. J. Phys. **76**(8), 750–757 (2008).
[8]Self-assembled quantum dots are not spherically symmetric. Rather, their size along one dimension (usually the direction of crystal growth) is much smaller than along the other two directions. Therefore, they can be well approximated as two-dimensional. For details, see, e.g., Ref. 7.
[9]W. Lei, O. Wibbelhoff, C. Notthoff, B. Marquardt, D. Reuter, A. D. Wieck, and A. Lorke, "Magnetic-field-induced modification of the wavefunctions in InAs quantum dots," Physica E **40**(6), 1870–1872 (2008).
[10]W. Lei, C. Notthoff, J. Peng, D. Reuter, A. Wieck, G. Bester, and A. Lorke, "'Artificial Atoms' in magnetic fields: wave-function shaping and phase-sensitive tunnelling," Phys. Rev. Lett. **105**, 176804 (2010).
[11]C. Cohen-Tannoudji, B. Diu, and F. Laloe, *Quantum Mechanics* (Wiley, Toronto, 1992), pp. 727–764.
[12]J. H. Davies, *The Physics of Low-Dimensional Semiconductors* (Cambridge U.P., Cambridge, 1998), Secs. 6.4 and 6.5.1.
[13]In analogy to atomic physics, the lowest electron shell in quantum dots is commonly called the "*s*-shell." Accordingly, the next-higher shell is called the *p*-shell, even for quantum dots, which do not have circular symmetry, so that angular momentum is no longer a good quantum number.
[14]Y. Tokura, S. Sasaki, D. G. Austing, and S. Tarucha, "Excitation spectra and exchange interactions in circular and elliptical quantum dots," Physica B **298**, 260–266 (2001).
[15]F. M. Peeters, "Magneto-optics in parabolic quantum dots," Phys. Rev. B **42**(2), 1486–1487 (1990).
[16]A. Beckel, D.-M. Zhou, B. Marquardt, D. Reuter, A. D. Wieck, M. Geller, and A. Lorke, "Momentum matching in the tunneling between 2-dimensional and 0-dimensional electron systems," Appl. Phys. Lett. **100**, 232110 (2012).
[17]R. J. Warburton, B. T. Miller, C. S. Dürr, C. Bödefeld, K. Karrai, J. P. Kotthaus, G. Medeiros-Ribeiro, P. M. Petroff, and S. Huant, "Coulomb interactions in small charge-tunable quantum dots: A simple model," Phys. Rev. B **58**(24), 16221–16231 (1998).